Prediction of the Timing and the Rhythm of the Parkinsonian Subthalamic Nucleus Neural Spikes Using the Local Field Potentials

Kostis P. Michmizos, *Member, IEEE*, Damianos Sakas, and Konstantina S. Nikita, *Senior Member, IEEE*

***Abstract*—In this paper, we discuss the use of a nonlinear cascade model to predict the subthalamic nucleus spike activity from the local field potentials recorded in the motor area of the nucleus of Parkinson's disease patients undergoing deep brain stimulation. We use a segment of appropriately selected and processed data recorded from five nuclei to acquire the information of the spike timing and rhythm of a single neuron and estimate the model parameters. We then use the rest of each recording to assess the model's accuracy in predicting spike timing, rhythm, and interspike intervals. We show that the cumulative distribution function (CDF) of the predicted spikes remains inside the 95% confidence interval of the CDF of the recorded spikes. By training the model appropriately, we prove its ability to provide quite accurate predictions for multiple-neuron recordings as well, and we establish its validity as a simple yet biologically plausible model of the intranuclear spike activity recorded from Parkinson's disease patients.**

***Index Terms*—Local field potential, nonlinear modeling, Parkinson's disease, subthalamic nucleus.**

I. Introduction

LOCATED deep inside the brain, the subthalamic nucleus (STN) plays a vital role in basal ganglia function and dysfunction. The STN is heavily related to the manifestation of the motor symptoms of spread neuro-degenerative pathologies and especially Parkinson's disease (PD) [1]. That is the reason why STN has become the main target in deep brain stimulation (DBS), i.e., the modulation of basal ganglia activity by direct electrical stimulation. Nonetheless, the underneath networking mechanisms of the STN are still partially known and the variety of firing patterns that the STN cells are able to produce [2] have not been reliably modeled yet. In addition, most of the existing experimentally verified models of the basal ganglia are pitched at a high level where the STN is either peripheral to the model (e.g., [3]–[5]) or its neuron types are heavily simplified ([6], [7]).

Manuscript received March 5, 2011; revised May 16, 2011; accepted May 20, 2011. Date of publication June 2, 2011; date of current version March 7, 2012.

K. P. Michmizos was with the Biomedical Simulations and Imaging Laboratory, Faculty of Electrical and Computer Engineering, National Technical University of Athens, 10682 Athens, Greece. He is now with the Massachusetts Institute of Technology, Cambridge, MA, USA (e-mail: konmic@mit.edu).

K. S. Nikita is with the Biomedical Simulations and Imaging Laboratory, Faculty of Electrical and Computer Engineering, National Technical University of Athens, 10682 Athens, Greece.

D. Sakas is with the Department of Neurosurgery, University of Athens, Evangelismos General Hospital, 10682 Athens, Greece (e-mail: sakasde@med.uoa.gr).

Digital Object Identifier 10.1109/TITB.2011.2158549

Neurophysiological activity, recorded during DBS, reflects the sum of action potentials (APs) from cells within approximately 50–350 μm from the tip of the recording electrode [8] and dendritic processes (resulting mainly from the influx or outflux of ions in the membrane of postsynaptic neurons) from within 0.5–3 mm from the tip of the recording electrode [9]. These two signal types can be segregated by frequency-band separation [10]: Specifically, using a high-pass filter cutoff of about 500 Hz and a low-pass filter cutoff of about 200 Hz, the spike activity and the so-called local field potentials (LFPs) can be obtained, respectively. A question then arises about whether the recorded intranuclear LFPs can be used to acquire the STN neurons' spike activity.

The prediction of neuronal firing from LFPs has been firstly examined in the primary visual cortical area (V1) of monkeys using extracellular microrecordings [11] and in the primary somatosensory cortical area (S1) of rats, using a combination of intracellular and extracellular recordings [12]. In [13], it has been demonstrated that some of the local properties of LFPs can be predicted by the spike activity of a few or even a single neuron. Until now, the predictive relation between LFPs and neuronal firing has been examined in the cortex of animals, mainly due to the accessibility of the area and the easiness of the surgical procedure. An effort to extend the LFP-spike relationship to a deep nucleus in monkeys was unsuccessful; almost no relation was found between the LFPs acquired from the dorsolateral area of the geniculate nucleus and the spike activity inside that nucleus [11].

In this paper, we propose a cascade model, inspired by the nonlinear nature of the spike generation process, to predict the individual STN spike timing and rhythm from the underlying LFPs. It is shown that the model is able to predict the neural activity with high to moderate accuracy, depending on the number of neurons present in the recording. From a neurocomputational point of view, given the central position of the STN in the basal ganglia system, the proposed model could serve as a test bed for pathophysiological and therapeutic theories. Such models are also heavily related to research studies on neural prostheses that aim to replace a damaged subregion of the brain (for a discussion see [14]). The rest of the paper is organized as follows. In Section II, an anatomical and physiological sketch of an STN neurons is drawn, followed by the experimental setup, and the signal processing applied to recordings presented in Section III. The methodology used to acquire the nonlinear model of the STN neuron is described in Section IV. In Section V, simulation results are used to validate the proposed model in terms

of spike timing and rhythm. The physiological implications of the obtained results and possible extensions of the model are discussed in Section VI.

II. Biological Foundation of the Model

A. STN Neuron Anatomy and Physiology

A projection neuron, found to be the principal type of an STN neuron, has rather long dendrites devoid of spines. Generally, projection neurons have four to nine dendrites radiating outwards, giving rise to tapering branches that extend beyond 400 μm [15]. The neurons are identical throughout the nucleus, i.e., STN is cytologically homogeneous [15]. The dendritic arborizations are ellipsoid, replicating in smaller dimension the STN's shape [16]. Cortical and thalamic afferents to the STN are glutaminergic [17] whereas pallidal afferents are GABAergic [17]. All afferents innervate the STN in a topographical manner. In monkeys and humans, there is a progressive bending of the dendrites along the nuclear limits [16]. Due to this bending, the STN can be regarded as a close nucleus, able to receive and process information from afferences which are specifically devoted to it. The direct targets of the STN are the pallidum [18] and both pars compact and pars reticulata of the substantia nigra [15]. The distribution of afferent projections from the globus pallidus external (GPe) and the selective distribution of the calcium binding proteins parvalbumin in neurons in the motor territory of the STN and calretinin in the associative and limbic territories suggest that the STN is divided into separate sensorimotor, associative, and limbic territories [19]. The dorsolateral part of the STN, projecting to the motor territory of the GPe [20], appears to represent the nucleus' motor territory. In conclusion, the motor area of the STN can be regarded as a neural area that is perfectly delimited, both anatomically and functionally.

B. Relationship Between LFP and Neurons' Input in the STN

LFPs are believed to be dominated by the more sustained currents in the tissue, typical of the somato-dendritic currents [21] with the major slow current being the postsynaptic potential (PSP). Yet it is also shown that LFPs are partly due to the existence of other types of slow activity unrelated to synaptic events, including voltage-dependent membrane oscillations [22] and spike afterpotentials [23]. Historically, research has been focused on LFPs in structures such as the cortex [24] and hippocampus [25]. The organized topography of such structures contributes to a relatively amplified and interpretable LFP signal. The significance of LFP signals recorded in areas where neurons are positioned in a less ordered manner is more controversial, leaving room for concern that LFPs recorded in structures like the STN may reflect to or be diluted by volume-conducted higher amplitude signals from structures outside the area of that nucleus [26]. Although some studies show that LFPs convey information that is to some degree independent of spike activity (e.g., [27]), it has been suggested and demonstrated by many studies that spikes synchronize to—or that synchronization gives rise to—specific oscillation frequencies of the LFPs, i.e., the γ-band ($>$40 Hz) in the visual cortex and the θ-band (4–8 Hz) in the hippocampus [28]. Using simultaneous recordings of LFPs and spikes, Mitzdorf [29] suggested that an LFP signal is more strongly correlated with excitatory PSPs, afterpotentials, and dendritic spikes than with spikes located close to the electrode neurons.

The basal ganglia do not share the laminar structure of the cortex. Yet, there is evidence that LFPs recorded in these nuclei also reflect synchronized aggregate activity [30]. This view is further supported by recent studies in Parkinsonian patients. Coupling has been demonstrated between single-unit and LFP recordings in STN [31]. In addition, oscillations in STN-LFPs are coupled to those in distant but connected sites, such as the GP and cerebral cortex, suggesting that they are at least partly associated with synchronized presynaptic and/or postsynaptic effects [32]. Thus, changes in LFPs within human STN are most probably informative about the aggregate activity of local neurons.

C. The STN Spike Activity as the Output Information

By placing a microelectrode sufficiently close to the membrane of a neuron, we can record the neuron's APs as a train of electrical impulses [33]. Electrophysiological research studies in the last 25 years have provided evidence that individual impulses in the impulse trains from each neural cell may sometimes be quite precisely timed and hence of great importance. For instance, impulse trains from single neurons may show above-chance recurrences of exactly timed sequences of several impulses [34]. There is also increasing evidence that such exact timing of impulses correlates with behavior [35] or with sensory analysis [36], and an increasing acceptance that exactly timed patterns of impulses may be of great significance in the information processing accomplished by the brain nuclei [37]. In addition to firing frequency, the firing pattern comprises several factors that include degree and duration of bursting activity, length of interburst pauses, and degree of temporal and spatial synchronization [37]. In conclusion, the neuron spike activity (in terms of spike rhythm and timing) is a valuable signal related to the output information sent inside and outside the nucleus.

III. Data Handling

A. Data Acquisition

A general scheme of our approach is shown in Fig. 1. Microelectrode recordings (MERs) were acquired during the surgical procedure [38] of implanting a DBS electrode within the motor area of STN in PD patients recruited from the Department of Functional Neurosurgery at Evangelismos General Hospital, Athens, Greece. MRI scans were performed the day prior to surgery to locate the motor area of the STN. The acquired images were co-registered with the frame based CT images acquired at the day of surgery (Neuroplan, Integra Radionics, Burlington, USA). Confirmatory MERs, lasting 10 s, were used to compensate for targeting errors related to unavoidable limitations (e.g., imaging resolution, brain anatomic shifts) of the surgical procedure. The exact target location was estimated by a neurologist during surgery, observing the neuronal activity recorded from

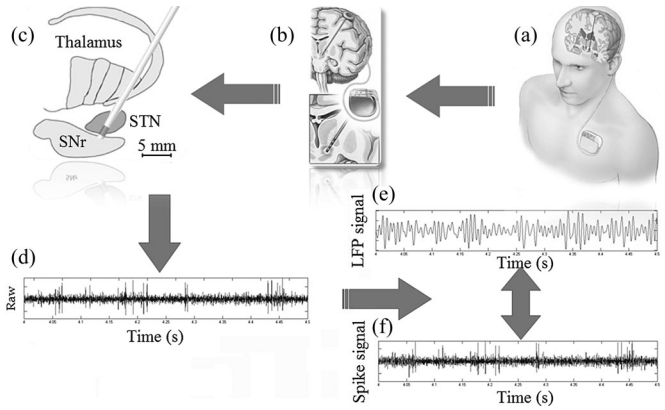

Fig. 1. Schematic representation of the process for acquiring the input and output signals of the proposed model. (a) The insertion of a DBS lead. (b) A zoomed-in version of the process. (c) Microelectrode positioned inside the STN. (d) Microelectrode recording (MER). (e) LFP signal (low-pass version of MER). (f) Spike signal (high-pass version of MER).

the nearby area, displayed on an oscilloscope and played on an audio monitor. A micropositioner system (Microtargeting Drive, Medtronic Inc., Minneapolis, MN) was used to advance recording microelectrodes in a controlled fashion, while measuring the exact depths. The system allowed the use of a 5-hole array which could accommodate five discrete channels at 2 mm distances, digitized at 24 kHz, through which the recording electrodes and later the DBS lead were inserted. In either case, multiple parallel trajectories were explored simultaneously, without making any changes in the stereotactic frame (Cosman–Roberts–Wells–Radionics Inc., Burlington, MA, USA) coordinates. Trajectories were positioned in a cross (Ben Gun) formation (central, anterior, posterior, lateral, and medial). MERs were acquired during spontaneous STN activity, defined as the neuronal activity acquired during periods in which the PD patient lied down immobile in the operational table, prior to DBS permanent lead implantation. MERs started at 5 mm above the intended target and allowed for a complete sampling of the neuronal activity of the STN. They were obtained at 1 mm steps through the STN to the substantia nigra reticulate (SNr) using the Leadpoint™ Neural Activity Monitoring System (Medtronic Inc., Minneapolis, MN).

B. Data Processing

Signals were visually inspected, and only epochs free from artifacts were processed. Recordings were visually examined for a typical STN discharge pattern (intense irregular neuronal activity with increased background activity and bursting spike trains usually present [39]). Off-line data processing and analysis was conducted using the MATLAB (The MathWorks, Natick, MA) code. Each digitized signal was low-pass filtered, using an equiripple filter with a cut-off frequency of 6 kHz, order of 900 and peak to peak (p-p) rippling equal to 1.6×10^{-5} dB and then downsampled to 12 kHz for computational convenience. To acquire the spike signal, we used an FIR generalized equiripple band-pass (BP) filter, of order of 2300 samples, with stop-bands of [0 450] Hz and [2.50 2.55] kHz, a pass-band of [0.5, 2.5] kHz and p-p rippling in pass-band equal to 2×10^{-6} dB. For acquiring the LFP signal, we used an FIR equiripple low-pass (LP) filter. The LP filter was chosen so that its order and p-p pass-band rippling would be equivalent to those of the BP filter. The filter had a pass-band of [0 200] Hz and a stop-band of [0.25 12] kHz. Finally, LFPs were normalized by dividing by twice the standard deviation of the LP filtered signals, in order to minimize variability within and among nuclei.

C. Spike Sorting

Using amplitude thresholding [40], we located the spikes in the recordings. K-means clustering via principal component analysis was applied to relate each spike to a specific neuron. Our data set included 16 single-neuron recordings (in which spikes from a second neuron were present in less than 5% of the whole recording) and 15 two-neuron and three-neuron recordings, acquired from five nuclei (three subjects). Regarding threshold selection, its absolute value was typically chosen equal to three times the SD of the distribution of all samples in the noisy spike signal, excluding the 1 ms spike segments. This means that a peak was considered as spike if its amplitude was almost 1.5 the noise level of the recorded signal (95% confidence interval). The threshold sign was also chosen based on the polarity of the signal (i.e., if the spike's highest amplitude was positive or negative). In some recordings, lowering the threshold near the noise level was necessary to detect some low-amplitude spikes, probably arriving from relatively remote neurons.

IV. Modeling the Spike Activity

A. Physiological Foundation of the Model

The generation of an AP is a strong nonlinear process since an abrupt change in the membrane potential precedes the opening or closing of ion channels. The model of the AP generation process was selected to be a linear time invariant (LTI) system (mainly representing the processes inside the cell body) followed by a nonlinear static module, used to describe the AP generation process. Such a system (Wiener system) has been widely used to model various physiological systems since its first introduction in 1972 [42]. In addition, until the recorded LFP signal reaches the cell's body, it is subject to voltage changes resulting from known and unknown dendritic processes. The voltage decrement was introduced into the model using a second nonlinear process before the Wiener system leading to the following Hammerstein–Wiener (H-W) model for the total process.

B. The Hammerstein–Wiener Model

In a H-W structure, a linear time invariant (LTI) dynamic block is preceded and followed by a static nonlinearity. In practice the H-W model is a special case of the Volterra–Wiener nonlinear models. Such a system's steady-state behavior is determined completely by the static nonlinearities, whereas its dynamic behavior is determined by both the nonlinearities and the linear dynamic model component. Briefly, if $k = n \cdot \Delta t$, $n \in N$ and Δt is the sampling period, a lumped parameter

H-W model is represented in the Z space by

$$v(k) = f(u(k)) \tag{1}$$

$$w(k) = \frac{a + bz^{-1} + \cdots + cz^{-n_b}}{a' + b'z^{-1} + \cdots + cz^{-n_f}} v(k) = \frac{B}{F} v(k) \tag{2}$$

$$y(k) = h(w(k)) \tag{3}$$

where $u \in R^m$ is the physical input (the LFP and noise) to the entry module of the model. The input is passed through the nonlinear mapping $f(u)$to give the input $v \in R^m$ of the linear dynamic block. In (2), *a,b,. . .c*, and *a′,b′,. . .,c′* are, respectively, the polynomial coefficients for the numerator, *B,* and the denominator, *F*, of the linear dynamic block, n_b is the order of B and n_f is the order of *F*. $w \in R^p$ is the output of the linear block which is passed through the nonlinear mapping *h(w)* to give the output $y \in \mathrm{R}^p$ of the model.

C. Parameter Estimation

We estimated recording-specific models. LFP-spike training pairs were acquired from the first 1 s of the recordings. Segments of the recordings between 1 and 2 s were used for visual validation. The last 8 s of the recordings were used for quantitative validation, as presented in Section V. No golden rule existed in terms of the order of the linear filter and the number of the nonlinear segments that produced the best prediction results. Each recording was handled separately to estimate the best model. We started with the simplest estimation (an autoregressive model with one pole) and we increased n_b and n_f (2) until satisfactory accuracy for the spikes was accomplished. A model that detected half of the spikes in the visual validation data segment without fabricating nonexistent spikes indicated the lower limit of a satisfactory prediction. he LTI order was kept as low as possible to allow the model to be able to generalize well especially across spikes arriving from different neurons. First-order statistics of the training LFP segments had to be comparable to the first-order statistics of the validation LFP segments. Usually, an LTI of orders $n_b \leq 2$ and $n_f \leq 2$ provided satisfactory prediction.

In single-neuron recordings, the model was identified using a training set of LFP-spike pairs (usually six to eight different pairs of 4–12 ms duration). In multiple-neuron recordings, the training set was composed of LFP-spike pairs in analogy to the spike rhythm of each neuron. Piecewise linear functions were used for both input and output nonlinearities of the H-W model. Due to the highly stochastic nature of the data, the piecewise linear representation differed significantly among models. The number of the line segments of the nonlinear estimators and the order of the linear model varied in predefined ranges. Usually 5 to 15 line segments were enough to estimate the nonlinear functions whereas the range of the poles and zeros of the LTI system was [0, 3]. A search method for iterative parameter estimation with one sample delay was applied to find the best possible combination of the parameters. The Gauss–Newton prediction error minimization was used when the input nonlinear function was invertible and the Levenberg–Marquardt search method was used when the input nonlinear function was singular.

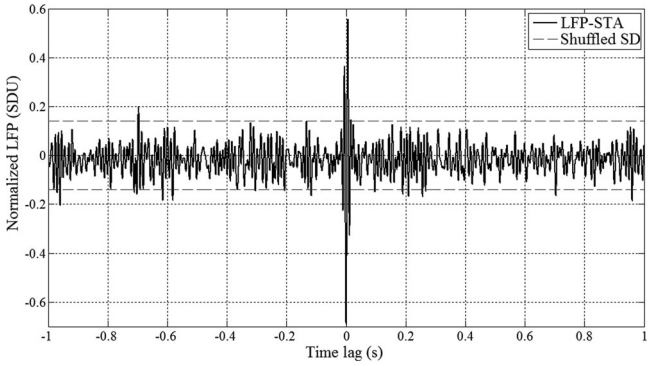

Fig. 2. STA of the STN LFP. Intranuclear recording (Subject 2, left STN, central electrode, 1 mm below theoretical target). For significance levels, ISIs are randomized and the SD of the resulting STA is calculated. Amplitude is in standard deviation units.

D. Performance Measures and Model Validation

Performance is quantitatively assessed using a plot of the empirical cumulative distribution function (CDF) of the detected spike times against the CDF of the predicted spike times. If the model accurately describes the observed spike data, then the empirical and model CDFs should roughly coincide, and the plot should follow a 45° line. A significant deviation from the 45° line reflects model's failure to account for some aspect of the spiking behavior. In addition, we assess the agreement between the model and data by constructing a sorted interspike interval (ISI) plot, which presents the predicted sorted ISIs against those acquired by the recording. These plots are used for visualizing which ISIs of the recorded data are well captured and which are poorly captured by the model. Such comparisons are useful in testing if the model predicts valuable characteristics of an STN neuron, such as the onset and the recession of a bursting spike train. Furthermore, the ability of the model to predict the timing and the duration of the spike bursts or, more generally, the spike rhythm of the recorded population of neurons is estimated as the number of spikes (predicted and recorded) in bins of 50 ms width.

V. Results

In this section, we first show the general spike-to-LFP relationship present in our data and then we report the model quantitative performance in terms of its ability to predict the area's spike trains from LFPs.

A. LFP-Spike Relationship

In order to measure local neuronal synchronization, we use the spike-triggered average (STA) of the LFP. Relationship between STN spike activity and the underlying LFPs is visualized in Fig. 2. Example recording is plotted. For the calculation of the STA, we obtain for each spike the LFP segment for a short time window (+/−1 s lag) around that spike and average over those LFP segments. Any components of the LFP that are not consistently phase locked to the spikes will average out and not be visible in the STA. If spike times had no temporal relation to the activity of surrounding neurons, fluctuations in the LFP

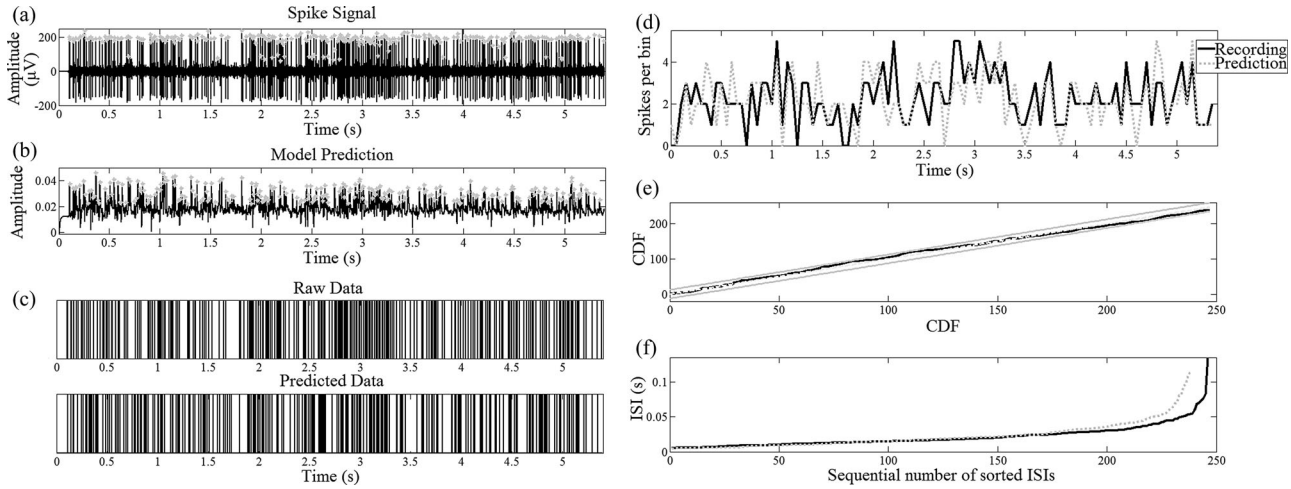

Fig. 3. (a) Raw recording. Spikes are marked with gray "x." (b) The model's output. Predicted spikes are marked with gray "x." (c) Raster plot for recorded and predicted data. (d) Spike rhythm estimated per 50 ms bin width. (e) CDF plot for the aforementioned prediction over the validation period. (f) Sorted ISIs for both predicted (dotted gray line) and recorded (thick black line) spike trains.

would average out during STA compilation, resulting in a flat STA. On the other hand, if spike times have a reliable temporal relation to the local neuronal activity as measured by the LFP, then LFP fluctuations add up during the spike triggered averaging process. Thus, the STA is very sensitive in detecting synchronization because the LFP averages over many spikes and neurons. The STA is equivalent to the cross correlation between the (white noise) input and the (sum of "deltas") output [41]. Since the STA has always a peak at zero lag, there is a linear relationship between the output (spikes) and the input (LFPs). Clearly, there is a linear relation between spikes and LFPs. In Fig. 2, one notes a sharp negativity at spike position at zero time lag and a prominent upswing for negative and positive time lags, i.e., right before and after spike has occurred. The negative spike in the STA as a response to spikes was common among electrodes and patients, provided that the signal came from an electrode inside the STN and that the spikes' peaks are above the noise level.

B. Models Estimated from Single-Neuron Recordings

In Fig. 3, a typical example of a predicted single-neuron spike train is presented. Raw recording [see Fig. 3(a)] was acquired from Subject 1 (male, 48-year old, UPDRS (off drugs) = 32), left STN, lateral electrode, 1.0 mm below the theoretical target. Some spikes arriving from a second neuron were detectable. The estimated H-W model had a linear time invariant (LTI) component of 1/(1-0.98z-1), and both its input and output nonlinear estimators were piecewise linear functions, with 20 linear segments. The output of the model [see Fig. 3(b)] comprised of spikes of various amplitudes. Spikes' amplitude was of no importance to our study; hence, each detected peak was translated as a predicted spike. A comparison between predicted and recorded signals, lacking the spike amplitude information, is given in a raster plot [see Fig. 3(c)]. The model predicted very accurately the overall structure of the recorded spike train, as seen from the estimated spike rhythm per 50 ms bin width [see Fig. 3(d)]. The exact onsets and offsets of the bursts were somewhat inaccurate in the prediction. However, even smaller bursts and single spikes were closely predicted, although no clear mark in the LFP signal could be seen with a naked eye. There were also occasions where spikes were simply missed (1.75 s – 1.85 s, 3.45 s – 3.55 s) or fabricated (1.6 s – 1.7 s, 2.55 s – 2.65 s). Nonetheless, in most of the cases, the model was able to predict the presence of both separate spikes and bursts with great accuracy. The CDF plot [see Fig. 3(e)] showed that the model displayed an accurate fit for the entire duration of the validation data. Model's output values lied in the border of the 95% confidence bounds. The maximum distance between model values and the 45° line was 11 spikes (at 1.6 s). A similar degree of discrepancy of the optimum models was found in almost half of single-neuron models (9 of 16). An excellent agreement between the ISI distribution of the recorded data and the predicted one was also observed [see Fig. 3(f)]. A slight discrepancy between the large values of ISIs means a somehow degraded ability of the model to detect the presence of a single spike after an extended absence of spikes. However, this was not always the case since 12 of 16 single-neuron models predicted the ISI accurately (mean squared error (MSE) was lower than 0.65 ms).

The ability of the model to predict the presence of a single spike or a burst of spikes depended on numerous factors. Such factors included the length of the LFP-spike training data pairs, the normalization process applied to the LFP signals and the order of the linear component as well as the number of the linear segments in the nonlinear estimators. The model's ability for accurate prediction increased with the length of the training pairs; yet, the length should be small enough to exclude the possibility of the presence of a second spike inside the training window.

C. Models Estimated from Multiple-Neuron Recordings

A few of the STN recordings included a single-neuron spike activity; the rest have spikes coming from multiple neurons. Therefore, a question arises on whether the identification

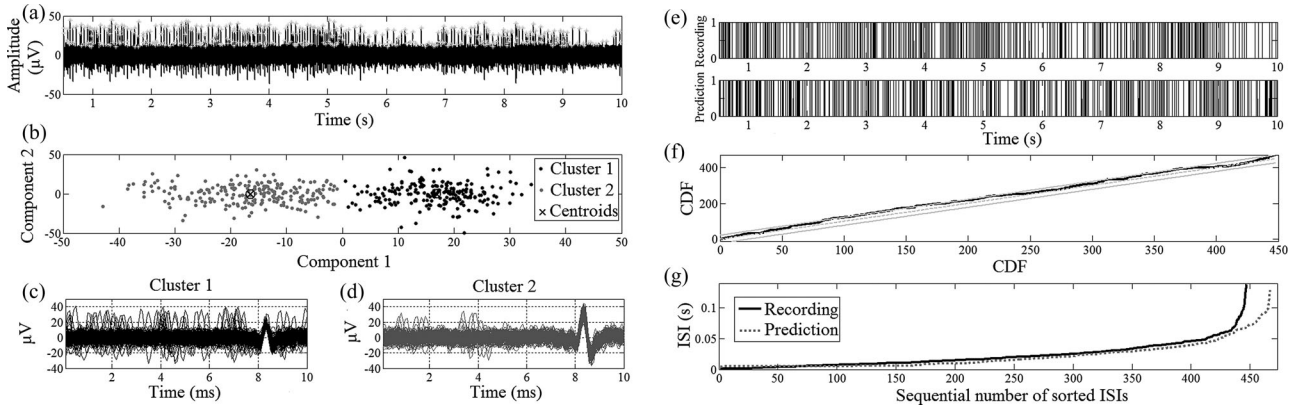

Fig. 4. (a) Spike data acquired from two-neuron recording. Spikes are marked with "x." (b) K-means PCA analysis on the spikes. (c)–(d) Spike clusters. (e) Raster plot for recorded (up) and predicted (down) spikes. (f) CDF plot for the above prediction over the validation period. (g) Sorted ISIs for predicted (dotted grey line) and recorded (thick black line) spike trains.

technique was able to create a model that could predict the spike activity of an "area" of neurons. In Fig. 4(a), an indicative example of a two-neuron recording is shown. Recording acquired from Subject 3 [male, 70-year old, UPDRS (off drugs) = 54]. Recording site: Left STN, posterior electrode, 1.5 mm before theoretical target. K-means algorithm returned a well separated set of two clusters [Fig. 4(b)]. The first had spike peaks slightly above the noise level [see Fig. 4(c)] and the other well above that level [Fig. 4(d)]. Visual inspection of the neural spikes belonging to each cluster verified correctness of clustering. In 9.5 s of the validation data segment for this recording, 448 spikes were detected in total. 215 spikes were clustered in the first group (22.6 spikes/s) and 233 spikes were positioned in the second group (24.5 spikes/s). The H-W model, estimated with 4 LFP-spike pairs from Cluster 1 and equal number of pairs from Cluster 2, was able to predict the spikes of both neurons [see Fig. 4(e)]. The predicted versus recorded CDF plot followed the 45° line quite accurately, sometimes approaching the 95% confidence bounds [Fig. 4(f)]. The maximum distance between model values and the 45° line was 22 spikes (at 1.3 s). The predicted ISI [Fig. 4(g)] also followed accurately the true ISI except for the large ISIs in which the model predicted the spikes with a short latency.

Cumulative results between the H-W models resulted from single-neuron recordings and those resulted from multineuron recordings showed quality degradation as the number of recorded neurons increased to more than one. The ISI predictability, as defined by the first-order statistics of the mean squared error (MSE), was in the mean sense degraded by 43% when we moved from single-neuron to multineuron recordings [Fig. 5(a)]. However, some of the multineuron models showed better performance than the average single-neuron modeling performance.

The spike rhythm was not altered significantly [Fig. 5(b)–(c)]. The mean MSE for multineuron rhythm predictions was increased by 29%, compared to the mean MSE for single-neuron rhythm, for bin width of 50 ms. However, this increase of the MSE was not only due to the inability of the model to predict the spikes accurately but it was also affected by the increase of the

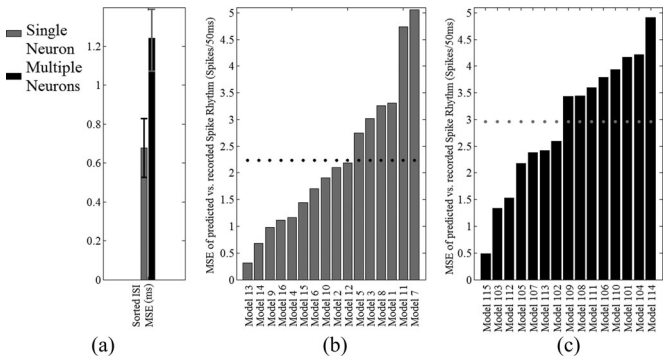

Fig. 5. Cumulative results for single-neuron and multineuron models. (a) MSE (in ms) between sorted recorded and predicted ISI curves. (b) MSE for single-neuron rhythm. Black dotted line represents the mean MSE for all single-neuron models. (c) Same as in (b), for multineuron recordings.

absolute number of the spikes per bin due to the firing of more than one neurons. This means that the multineuron models did not perform as well as the single-neuron models, in terms of the exact timing of each spike, yet their rhythm predictability was still comparable with the rhythm predictability of single-neuron models.

VI. Conclusion

We introduced a physiologically plausible nonlinear cascade model for predicting an output temporal pattern of AP events as a function of an input electrophysiological pattern of LFPs for an STN neuron. Methods from nonlinear system identification theory were used to address the inherently nonlinear mechanisms underlying neural firings. The approach was demonstrated to be successful when it was also applied to multineuron STN train data recorded. The proposed model aims to understand the basic information produced by a small neural area inside STN. However, understanding how STN processes information requires understanding how temporal patterns of activity are formed.

If the simultaneous recording at various depths inside the STN becomes technologically feasible and medically justifiable, a 3D neurophysiological model of the intranuclear spike activity would also be able to be inferred from the recordings. Another

important extension of the proposed modeling approach is to allow for a physiologically justified alternation of the model's input and compare the output with certain known pathophysiological patterns of the neural behavior. For example, it is widely shown that STN DBS causes a significant attenuation in power in the beta band of LFPs at rest. By changing appropriately the model's input, different theories of the DBS effect on the LFP could be tested. By allowing for high-level functional views that are still consistent with low level ideas of operation, the proposed model can be used as a test bed for current and future theories on the STN and even shed some light on the effect that DBS has on the STN function.

REFERENCES

[1] P. Limousin, P. Pollak, A. Benazzouz, D. Hoffmann, J. F. Le Bas, E. Broussolle, J. E. Perret, and A. L. Benabid, "Effect of parkinsonian signs and symptoms of bilateral subthalamic nucleus stimulation," *Lancet*, vol. 345, pp. 91–95, 1995.

[2] J. I. Kass and I. M. Mintz, "Silent plateau potentials, rhythmic bursts, and pacemaker firing: Three patterns of activity that coexist in quadristable subthalamic neurons," *Proc. Natl. Acad. Sci. U.S.A.*, vol. 103, no. 1, pp. 183–188, 2006.

[3] W. Schultz, "Predictive reward signal of dopamine neurons," *J. Neurophysiol.*, vol. 80, pp. 1–27, 1998.

[4] T. Prescott, K. Gurney, F. Montes-Gonzalez, M. Humphries, and P. Redgrave, "The robot basal ganglia: action selection by an embedded model of the basal ganglia," in *The Basal Ganglia,* vol. 7, L. Nicholson and R. Faull, Eds. New York: Kluwer Academic, 2002, pp. 349–358.

[5] G. Tsirogiannis, A. Tagaris, D. Sakas, and K. S. Nikita, "A population level computational model of the basal ganglia that generates parkinsonian local field potential activity," *Biological Cybern.*, vol. 102, pp. 155–176, 2010.

[6] A. Gillies and D. Willshaw, "A massively connected subthalamic nucleus leads to the generation of widespread pulses," *Proc. R. Soc. Lond. B*, vol. 265, pp. 2101–2109, 1998.

[7] K. S. Nikita and G. L. Tsirogiannis, "Computational models simulating electrophysiological activity in the basal ganglia," *Acta Neurochirurgica Supplementum*, vol. 97, no. 2, pp. 505–511, 2007.

[8] A. D. Legatt, J. Arezzo, and H. G. Vaughan, "Averaged multiple unit activity as an estimate of phasic changes in local neuronal activity: Effects of volume-conducted potentials," *J. Neurosci. Methods*, vol. 2, pp. 203–217, 1980.

[9] U. Mitzdorf, "Properties of the evoked-potential generators: Current source-density analysis of visually evoked-potentials in the cat cortex," *Int. J. Neurosci.*, vol. 33, pp. 33–59, 1987.

[10] N. Logothetis, "The neural basis of the blood-oxygen-level-dependent functional magnetic resonance imaging signal," *Philos. Trans. R. Soc. Lond. B Biol. Sci.*, vol. 357, pp. 1003–1037, 2002.

[11] M. Rasch, A. Gretton, Y. Murayama, W. Maass, and N. Logothetis, "Inferring Spike Trains From Local Field Potentials," *J. Neurophysiol.*, vol. 99, pp. 1461–1476, 2008.

[12] M. Okun, A. Naim, and I. Lampl, "The subthreshold relation between cortical local field potential and neuronal firing unveiled by intracellular recordings in awake rats," *J. Neurosci.*, vol. 30, pp. 4440–4448, 2010.

[13] M. Rasch, N. Logothetis, and G. Kreiman, "From neurons to circuits: linear estimation of local field potentials," *J. Neurosci.*, vol. 29, pp. 13785–13796, 2009.

[14] M. Lebedev and M. Nicolelis, "Brain–machine interfaces: Past, present, and future," *Trends Neurosci.*, vol. 29, pp. 536–546, 2006.

[15] M. Carpenter, "Anatomy of the corpus striatum and brainstem integrating systems," *Handbook Physiol. Nerv. Syst.*, vol. 2, pp. 947–995, 1981.

[16] J. Yelnik and G. Percheron, "Subthalamic neurons in primates: a quantitative and comparative anatomy," *Neuroscience*, vol. 4, no. 11, pp. 1717–1743, 1979.

[17] M. Bevan, C. Francis, and J. Bolam, "The glutamate-enriched cortical and thalamic input to neurons in the subthalamic nucleus of the rat: Convergence with GABA-positive terminals," *J. Comp. Neurol.*, vol. 361, pp. 491–511, 1995.

[18] M. Bevan, A. Crossman, and J. Bolam, "Neurons projecting from the entopeduncular nucleus to the thalamus receive convergent synaptic inputs from the subthalamic nucleus and the neostriatum in rat," *Brain Res.*, vol. 659, pp. 99–109, 1994.

[19] J. C. Levesque and A. Parent, "GABAergic interneurons in human subthalamic nucleus," *Movement Disorders*, vol. 20, no. 5, pp. 574–584, 2005.

[20] V. Mark and E. Benarroch, "Subthalamic nucleus and its connections: Anatomic substrate for the network effects of deep brain stimulation," *Neurology*, vol. 72, no. 12, p. 1110, 2009.

[21] J. S. Buchwald, E. Hala, and S. Schramm, "A comparison of multi-unit activity and EEG activity recorded from the same brain site in chronic cats during behavioral conditioning," *Nature*, vol. 205, pp. 1012–1014, 1965.

[22] A. Kamondi, L. Acsady, X. Wang, and G. Buzsaki, "Theta oscillations in somata and dendrites of hippocampal pyramidal cells *in vivo:* Activity-dependent phase-precession of action potentials," *Hippocampus*, vol. 8, pp. 244–261, 1998.

[23] M. Kobayashi, T. Inoue, R. Matsuo, Y. Masuda, O. Hidaka, Y. Kang, and T. Morimoto, "Role of calcium conductances on spike afterpotentials in rat trigeminal motoneurons," *J. Neurophysiol.*, vol. 77, pp. 3273–3283, 1997.

[24] S. N. Baker, E. Olivier, and R. N. Lemon, "Coherent oscillations in monkey motor cortex and hand muscle EMG show task-dependent modulation," *J. Physiol.*, vol. 501, pp. 225–241, 1997.

[25] G. Buzsaki, "Theta rhythm of navigation: Link between path integration and landmark navigation, episodic and semantic memory," *Hippocampus*, vol. 15, pp. 827–840, 2005.

[26] J. R. Walters, D. Hu, C. A. Itoga, L. C. Parr-Brownlie, and D. A. Bergstrom, "Do local field potentials reflect synchronized spiking activity of neuronal populations in the basal ganglia? Studies in a rodent model of Parkinson's disease," in *The Basal Ganglia*, vol. 8, J. P. Bolam, C. Ingham, and P. J. Magill, Eds., 2005, pp. 37–46, Available: http://www.springerlink.com/content/tw7717k532217g4j/.

[27] G. Kreiman, C. P. Hung, A. Kraskov, R. Q. Quiroga, T. Poggio, and J. J. DiCarlo, "Object selectivity of local field potentials and spikes in the macaque inferior temporal cortex," *Neuron*, vol. 49, pp. 433–445, 2006.

[28] G. Buzsáki, *Rhythms of the Brain*. Oxford: Oxford Univ. Press, 2006.

[29] U. Mitzdorf, "Current source-density method and application in cat cerebral cortex: Investigation of evoked potentials and EEG phenomena," *Physiol. Rev.*, vol. 65, pp. 37–99, 1985.

[30] T. Tsubokawa and J. Sutin, "Pallidal and tegmental inhibition of oscillatory slow waves and unit activity in the subthalamic nucleus," *Brain Res.*, vol. 41, pp. 101–108, 1972.

[31] R. Levy, P. Ashby, W. Hutchison, A. Lang, A. Lozano, and J. Dostrovsky, "Dependence of subthalamic nucleus oscillations on movement and dopamine in Parkinson's disease," *Brain*, vol. 125, pp. 1196–1209, 2002.

[32] P. Brown, P. Mazzone, A. Oliviero, M. G. Altibrandi, F. Pilato, P. A. Tonali, and V. Di Lazzaro, "Effects of stimulation of the subthalamic area on oscillatory pallidal activity in Parkinson's disease," *Exp. Neurol.*, vol. 188, pp. 480–490, 2004.

[33] C. M. Gray, P. E. Maldonado, M. Wilson, and B. McNaughton, "Tetrodes markedly improve the reliability and yield of multiple single-unit isolation from multi-unit recordings in cat striate cortex," *J. Neurosci. Methods*, vol. 63, pp. 43–54, 1995.

[34] J. E. Dayhoff and G. L. Gerstein, "Favored patterns in spike trains: II," *Appl. J. Neurophysiol.*, vol. 49, pp. 1349–1363, 1983.

[35] A. E. P. Villa, "Empirical evidence about temporal structure in multi-unit recordings," in *Time and the Brain. (Conceptual Advances in Brain Research series)*, R. Miller, Ed. London: Harwood Academic Publishers, 2000, pp. 1–51.

[36] J. W. McClurkin and L. M. Optican, "Primate striate and prestriate cortical neurons during discrimination. I. Simultaneous temporal encoding of information about color and pattern," *J. Neurophysiol.*, vol. 75, pp. 481–495, 1996.

[37] C. F. Stevens and A. Zador, "Neural coding: The enigma of the brain," *Curr. Biol.*, vol. 5, pp. 1370–1371, 1995.

[38] D. E. Sakas, A. T. Kouyialis, E. J. Boviatsis, I. G. Panourias, P. Stathis, and G. Tagaris, "Technical aspects and considerations of deep brain stimulation surgery for movement disorders," *Acta. Neurochir. Suppl.*, vol. 97, pp. 163–170, 2007.

[39] M. Bevan, P. Magill, D. Termanc, J. Bolamb, and C. Wilsond, "Move to the rhythm: oscillations in the subthalamic nucleus—external globus pallidus network," *Trends Neurosci.*, vol. 25, no. 10, pp. 525–531, 2002.

[40] M. S. Lewicki, "A review of methods for spike sorting: The detection and classification of neural action potentials," *Network: Computation Neural Syst.*, vol. 9, pp. R53–R78, 1998.

[41] V. Z. Marmarelis and K. I. Naka, "White-noise analysis of a neuron chain: An application of the Wiener theory," *Science*, vol. 175, pp. 1276–1278, 1972.
[42] F. Rieke, D. Warland, R. de Ruyter van Steveninck, and W. Bialek, *Spikes Exploring the Neural Code*. Cambridge: MIT Press, 1997, pp. 289–295.

Konstantinos (Kostis) Michmizos (S'09–M'12) received the five-year Diploma in computer engineering and informatics from the University of Patras, Patras, Greece, in 2004, the M.Eng. degree in biomedical engineering from McGill University, Montreal, Canada, in 2006, and the Ph.D. degree from the Department of Electrical and Computer Engineering, National Technical University of Athens, Athens, Greece in 2011.

He is currently a Postdoctoral Associate at the Massachusetts Institute of Technology, Cambridge. He is the first author of 17 papers published in refereed international journals and conference proceedings. He has participated as a Research Assistant in Greek and EU funded projects. His research interests include the motor system of the human brain in terms of analyzing neuronal signals, identifying neural systems and controlling robotic devices for rehabilitation purposes.

Dr. Michmizos is the recipient of 11 awards and scholarships from foundations in Greece and Canada including the Onassis Foundation Scholarship (twice), the State Scholarship Foundation, and the Award from the Technical Chamber of Greece for excellent academic performance. He is a founder member of the Greek Society for Occupational Therapy, Exercise and Rehabilitation, a member of the Technical Chamber of Greece since 2006, and was a Treasurer in the IEEE Engineering in Medicine and Biology Society Greece Chapter from 2009 to 2010.

Damianos Sakas received the Graduate degrees from the Ioannidios School of Piraeus, Piraeus, Greece, in 1972, and Medical School, University of Athens, Athens, Greece, in 1978.

He was a Consultant Neurosurgeon at Walsgrave Hospital, Coventry, U.K., in 1993, the Midland Centre for Neurology and Neurosurgery, University of Birmingham, U.K., in 1994, and the University Hospital Coventry and Warwickshire, U.K., from 1995 to 1999. He was an Honorary Senior Clinical Lecturer at the University of Warwick, U.K., from 1995 to 1999, and a Lead Clinician in the Department of Neurosciences, University Hospital Coventry and Warwickshire from 1997 to 1999. Since 2000, he has been a Professor of Neurosurgery and the Chairman of the Department of Neurosurgery, University of Athens, Evangelismos General Hospital, Athens. His special neurosurgical interests include epilepsy surgery, movement disorders surgery, vascular surgery, neurotrauma, skull base surgery, and neuromodulation.

Konstantina S. Nikita (M'96–SM'00) received the Diploma in electrical engineering and the Ph.D. degree from the National Technical University of Athens (NTUA), Athens, Greece in 1986 and 1990, respectively. She received the M.D. degree from the Medical School, University of Athens, in 1993.

From 1990 to 1996, she was a Researcher at the Institute of Communication and Computer Systems, NTUA. In 1996, she joined the School of Electrical and Computer Engineering, NTUA, as an Assistant Professor, where she has been a Professor since 2005.. Her current research interests include biomedical signal and image processing and analysis, biomedical informatics, simulation of physiological systems, medical imaging, biological effects, and medical applications of radiofrequency electromagnetic fields. She has authored or co-authored 160 papers in refereed international journals and chapters in books, and more than 280 papers in international conference proceedings. She is author or co-author of two books: *Simulation of Physiological Systems and Medical Imaging Systems* (in Greek) and co-editor of one book: *Computational Electromagnetics: State of the Art and Future Trends* (Berlin, Germany: Springer, in English). She holds two patents. She has been the technical manager of several European and National Research and Development projects in the field of biomedical engineering.

Dr. Nikita has been honorary chair/chair/member of the program/organizing committee of more than 70 international conferences on the same fields (IEEE-IST, IEEE-BIBE, IEEE-ITAB, ICST-Mobihealth, etc.). She has served as a keynote/invited speaker at several international conferences, symposia, and workshops organized by NATO, WHO, ICNIRP, IEEE, URSI, COMCON, PIERS, etc. She is an Editorial Board Member of the IEEE TRANSACTIONS ON BIOMEDICAL ENGINEERING and an Guest Editor of several international journals on biomedical engineering subjects (IEEE TRANSACTIONS ON INFORMATION TECHNOLOGY IN BIOMEDICINE, Computerized Medical Imaging and Graphics, IOP Measurement Science and Technology, etc). She has been the Advisor of 20 completed Ph.D. theses, several of which have received various awards. She has served as external evaluator in numerous University promotion committees and in international and national committees for grant proposal applications. She has received various honors/awards, among which, the prestigious Bodossakis Foundation Academic Prize for exceptional achievements in "Theory and Applications of Information Technology in Medicine" (2003). She has been a member of the Board of Directors of the Hellenic National Academic Recognition and Information Center, a member of the Board of Directors of the Greek Atomic Energy Commission, and a member of the National Council of Research and Technology. She is a member of the Technical Chamber of Greece and a member of the Athens Medical Association. She is also the Founding Chair and Ambassador of the IEEE Engineering in Medicine and Biology Society, Greece Chapter, the Vice Chair of the IEEE Greece Section, and the Deputy Head of the School of Electrical and Computer Engineering of the NTUA.